ULTRASONIC IMAGING **32,** 16- 32 (2010)

# Small Lesion Detection with Resolution Enhancement Compression

PAUL LINDEN,[1] JOSE R. SANCHEZ[2] AND MICHAEL L. OELZE[1]

[1]*Beckman Institute*
*405 N. Mathews*
*Urbana, Illinois 61801*
*oelze@illinois.edu*

[2]*Bradley University*
*1501 W. Bradley Avenue*
*Peoria, IL 61625*

A novel coded-excitation method, resolution-enhancement compression (REC), increases the axial resolution and the echo signal-to-noise ratio (eSNR) for an ultrasonic imaging system. The REC technique was examined for its ability to improve lesion detectability. The REC technique was used to double the –3-dB fractional pulse-echo bandwidth of an ultrasonic source in both simulations and experiments. The increase in usable bandwidth increased lesion detectability compared to conventional pulsing (CP) techniques and coded excitation using a linear chirp (LC). Lesion detectibility was quantified through lesion signal-to-noise ratio (lSNR), which is a metric that quantifies the ability of an isolated observer to detect a focal lesion against a background. In simulations, a higher lSNR value was observed using the REC technique for lesions ranging in size from 1 mm to 8 mm in diameter. In addition, the eSNR was increased by almost 15 dB. To validate simulation results, a hydrogel-cone phantom was constructed to provide lesions with +6-dB contrast of different sizes. A transducer was scanned perpendicular to the major axis of the cone at different levels to provide lesions of 3, 5 and 8 mm in diameter. The lSNR was estimated for lesions of different sizes and using the three excitation techniques, i.e., CP, LC and REC. In experiments, the lSNR was observed to be higher using the REC technique than the other pulsing techniques. The lSNR scores for REC were higher by 15%, 45% and 40% for the 3, 5 and 8 mm over the other two excitation techniques. The eSNR was increased by 5.7 dB. Therefore, accrding to the lSNR metric, the improvement in spatial resolution from the REC technique resulted in improved detectability of small lesions.

KEY WORDS: Coded excitation; lesion signal-to-noise ratio (lSNR); pulse compression; resolution enhancement compression (REC); Wiener filter**.**

## I. INTRODUCTION

Improving image quality in a diagnostic ultrasound system is a natural goal. Image quality in ultrasound systems can be characterized by contrast resolution, echo signal-to-noise ratio (eSNR) and spatial resolution. Contrast resolution can be quantified through the contrast-to-noise ratio (CNR). Typically, contrast between soft tissues is low compared to other imaging modalities. The reflectivity between tissue interfaces can be as low as 1 part in $10^6$.[1] The impedance mismatch between tissue structures results in the reflection or scattering of ultrasound and it is this reflected ultrasound that is used to produce images. Scattering of sound from objects can be classified into three broad categories: specular, diffractive and diffusive.[2] Specular refers to scattering from objects much larger than the wavelength; diffractive to objects about the same size as the wavelength; and diffusive to objects much smaller than a wavelength. The speckle in biomedical ultrasound images results from scattering from objects smaller than a wavelength. This scattering is deterministic and cannot be removed by time averaging of the signal. However, information about the subwavelength scatterers can be inferred from the backscattered ultrasound.[3]



0161-7346/10 $18.00

While the speckle in the ultrasound image correlates to information about subwavelength scatterers, it can degrade the ability of an ultrasound system to detect low-contrast targets or small lesions.[1] Detection of lesions against a background is of prime importance in medical imaging. Examples include the detection of breast masses, focal lesions in the liver or infarcted regions of myocardium.[4] Therefore, much research has been conducted to quantify the detectability of targets using ultrasound imaging and to improve target detection through various mechanisms, e.g., speckle reduction.[5]

Much of the framework for quantifying target detectability in biomedical ultrasound was established by Wagner and colleagues.[1,4,6] Smith et al derived contrast/detail curves as a function of contrast, resolution cell volume and lesion diameter.[4] Interestingly, they found contrast/detail analysis curves for enveloped-detected ultrasound images were nearly identical to the square-law detector (those used with lasers). Smith et al noted that these contrast/detail curves suggested that lesion contrast was dependent on lesion diameter at the observer's threshold for lesion detection.[4] Such curves could be used to predict the performance of an imaging system with respect to lesion detection before performing extensive clinical trials in order to yield receiver-operator-characteristics (ROC) curves.

In addition to the contrast/detail analysis, another metric of paramount importance in any imaging modality is the eSNR. If eSNR decreases, noise begins to dominate the signal and, consequently, CNR is reduced as the image is washed out with noise. Conversely, as eSNR is increased, a better CNR may be achievable, resulting in increased lesion detectibility.

Scanners that function with a traditional pulse/echo excitation scheme are limited by pulse duration and peak pressure values, which can also limit the eSNR. The axial resolution of a pulse/echo system is related to the length of the transmitted pulse and peak-pressure is limited by the hardware of the system or by FDA regulations. If the pulse length is appreciably shortened without increasing peak pressure, eSNR can decrease, which may result in a reduction in image quality.

One method for boosting the eSNR is through coded-excitation techniques. Coded excitation has been used for decades in radar systems.[7] Takeuchi first proposed coded excitation for biomedical ultrasonic imaging in 1979 in a technique called the spread-energy method (i.e., FM chirps and phase coding).[8] However, ultrasonic imaging systems are limited by much smaller bandwidths than radar systems. Therefore, Takeuchi suggested that the only increase in the time-bandwidth product (TBP) comes from increasing the period of the transmitted signal, because the bandwidth of the system was already taken to the limit.

Coded excitation combined with pulse compression is a method that decouples the dependence of axial resolution on pulse length. The axial resolution of a short-duration pulse can be approximated as $=1/B$, where $B$ represents the bandwidth of the system and is the temporal resolution.[9] The bandwidth of a system is largely limited by the passband nature of the transducer. A typical pulse will have a TBP of approximately unity.[10] Coded excitation includes a broad class of signals with a TBP greater than unity. The TBP quantifies the difference between a single carrier and a coded-excitation waveform. Thus, a longer signal of desired power and bandwidth can be constructed without a major loss in axial resolution. The longer transmit signal is compressed on receive to restore axial resolution.

Pulse compression can be achieved by inverse filtering, matched filtering or mismatched filtering, e.g., a Wiener filter. The method of compression used dictates the eSNR, the maximum sidelobe levels and the compressed pulse length. Sidelobes are a byproduct of pulse compression that can degrade image quality by returning on-axis echoes, which appear as ghost images. Conventional pulsing schemes do not suffer from sidelobes. If not carefully constructed, sidelobes from pulse compression of codes can be as high as 13.2 dB (sidelobes of the sinc function). A reasonable expectation is to require maximum range sidelobe levels to be lower than the dynamic range of the ultrasonic imaging system, which typically oper-

ates at dynamic ranges greater than 45 dB.[11] Misaridis and Jensen claimed to achieve range sidelobe suppression between 60 to 100 dB.[9] The method used to achieve such low sidelobe suppression was amplitude or phase predistortion in addition to mismatch filtering.

Several researchers have investigated coded excitation/pulse compression techniques for ultrasonic imaging systems with promising results.[9-14] The most common waveforms in this class of signals are pulse modulation (PM), linear frequency modulation (LFM) and nonlinear frequency modulation (NLFM) signals. Coded-excitation waveforms in ultrasound can be optimized to produce improved image quality. A few desirable characteristics of an ultrasound waveform before compression are a large time-bandwidth product, short-duration and low sidelobes upon compression. However, an excitation waveform of significantly longer duration is still undesirable because it can reduce frame rate and the excitation pulse can overlap with echo returns. The frame rate can be reduced because as the pulse length is significantly extended, the interpulse interval (pulse repetition frequency or prf) must also be extended. A reduction in the prf will directly reduce frame rate.

A novel coding technique that improves not only the eSNR but also results in an improved axial resolution is the resolution-enhancement compression (REC) technique.[12] REC boosts energy in the transition bands of the transducer impulse response, consequently doubling the usable bandwidth, improving the resolution and improving the eSNR. REC was observed to boost system bandwidth by as much as 100% over conventional pulsing techniques. In addition, REC improved eSNR and spatial resolution (measured with the modulation transfer function (MTF)) in simulations and experiments.[12] The MTF quantifies how well an imaging system delivers contrast at different spatial frequencies. Furthermore, long range sidelobe levels were reported to be  45 dB.

The REC technique was also combined with frequency compounding (FC) to increase the tradeoff between spatial resolution and contrast.[13] Frequency compounding is a method of averaging images created from partially-uncorrelated subbands to reduce speckle interference and increase contrast. However, it also degrades axial resolution because each subband is a fraction of the original bandwidth. By combining REC with FC, contrast was improved by reducing speckle variance while maintaining the original bandwidth of the imaging system. Sanchez and Oelze claimed to achieve increases in CNR by as much as 231% over CP with subbands of 50% of the original transducer bandwidth.[13]

In addition, the REC technique was also combined with quantitative ultrasound (QUS) imaging to estimate the effective scatterer diameter.[14] This technique, called REC-QUS, increased contrast of scatterer diameter images by 51%. In addition, REC-QUS decreased the standard deviation of effective scatterer diameter estimates by 60% in simulations. In experiments, REC-QUS was observed to reduce the standard deviation of effective scatterer diameter estimates by 34% to 71%.

Lesion detectability is a function of the contrast between lesion background, lesion size, speckle variance and spatial resolution of the imaging system. Because REC provides an improvement in the spatial resolution and eSNR, improvements in the detectability of small lesions should follow. In the current study, the REC technique will be examined for its ability to improve target detectability, specifically, small lesion detectability.

## II. METHODS

### A. REC

REC is a coded excitation/pulse compression scheme that boosts the energy in the transition bands of the transducer. The bandpass nature of the transducer normally attenuates fre-

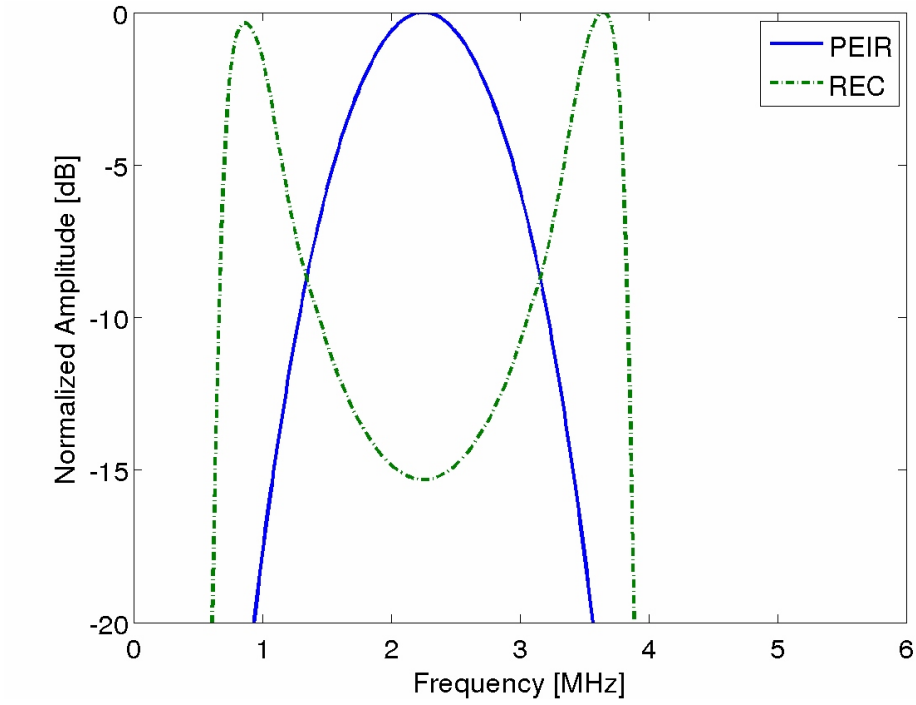


**FIG. 1** Transducer pulse/echo impulse response (PEIR) and a REC excitation waveform.

quencies in the transition band. By boosting the energy in the transition band with respect to the center frequency of the transducer, a larger usable bandwidth can be achieved. This boost in the transition bands is illustrated in figure 1. A physical description of REC is the boosting of the frequencies on the edges of the transducer spectrum. The result is a higher useable bandwidth that is far enough above the noise floor for imaging.

Consider the impulse response of a bandlimited transducer to be $h_1(t)$ and a desired impulse response, $h_2(t)$, of a second hypothetical transducer with a larger fractional bandwidth than $h_1(t)$. Let $v_{lin}(t)$ be a LFM chirp matched to the desired impulse response, $h_2(t)$, and let $v_{pre}(t)$ be a yet-to-be determined pre-enhanced chirp used to excite the actual transducer with the impulse response, $h_1(t)$. The output of a transducer excited with a code is the coded waveform convolved with the impulse response. Let $c_1(t)$ and $c_2(t)$ represent the output of these respective convolutions,

$$\begin{matrix} h_1(t) & 0 & v_{pre}(t) & c_1(t) \\ 0 & h_2(t) & v_{lin}(t) & c_2(t) \end{matrix}. \tag{1}$$

By setting $c_1(t)$ and $c_2(t)$ equal, the pre-enhanced chirp can be solved for by applying the theory of convolution equivalence to the following system,

$$h_1(t) \quad v_{pre}(t) \quad h_2(t) \quad v_{lin}(t). \tag{2}$$

By solving Eq. (2) in the frequency domain, a more simplified expression can be solved for:

$$V_{PRE}(f) \quad \frac{V_{LIN}(f) \quad H_2(f)}{H_1(f)}. \tag{3}$$

To avoid dividing by zero, a modified inverse can be used, [12]

$$V_{PRE}(f) \quad V_{LIN}(f) \quad H_2(f) \quad \frac{H_1^*(f)}{\left|H_1(f)\right|^2 \quad \left|H_1(f)\right|^2}. \tag{4}$$

In practice, the transducer will be excited by a pre-enhanced chirp found through convolution equivalence and then compressed with the linear chirp $v_{lin}(t)$, to obtain $h_2(t)$. Moreover, the desired impulse response, $h_2(t)$, can be constructed to have properties desirable for an imaging system such as a large fractional bandwidth. Figure 2 shows this sequence in the time domain and figure 3 is the frequency-domain equivalent.

The impulse response convolved with a pre-enhanced chirp (Fig. 2c) is equivalent to the desired impulse response convolved with the linear chirp (Fig. 2f) by convolution equivalence. Therefore, if the actual transducer is excited by a pre-enhanced chirp, a compression method can be designed with $v_{lin}(t)$ that will result in a higher-bandwidth imaging system. The linear chip is matched to a transducer impulse response by setting the bandwidth of the linear chip to the optimum bandwidth of the transducer, i.e., defined as 1.14 times the 6 dB bandwidth of the transducer.[15] A linear chirp can be expressed as[9]

$$v_{lin}(t) \quad w(t)\exp \quad j2 \quad f_0 \quad \frac{B}{2} \quad t \quad \frac{B}{2T_P}t^2 \quad ,0 \quad t \quad T_P, \tag{5}$$

where $f_0$ represents the center frequency and $B/T$ represents the FM sweep or frequency ramp constant. The parameter $B$ represents the total bandwidth that will be swept, which is [$f_0$-$B/2$,$f_0$+$B/2$], and $w(t)$ is a windowing function. The parameter $T_P$ is time period of the chirp. The FM linear chirp can be represented in discrete frequency as

$$v_{lin}[n] \quad w[n]\exp \quad j2 \quad f_0 \quad \frac{B}{2} \quad \frac{n}{f_s} \quad \frac{B}{2T_P} \quad \frac{n}{f_s}^2 \quad ,0 \quad n \quad T_P \Big/ f_s. \tag{6}$$

In Eq. (6) the continuous parameter $t$ has been replaced by the discrete integer $n$ and $f_s$ represents the sampling frequency. The window function, $w[n]$, is a pretransmission smoothing parameter that helps lower range lobes upon compression. The windowing function used was the Tukey window with 8% taper[12]

$$w[n] \quad \begin{cases} 1, & 0 \quad |n| \quad \frac{N}{2} \quad 1 \\ 0.5 \quad 1.0 + \cos \quad \frac{n - \frac{N}{2} \quad 1}{N \quad 1}, & \frac{N}{2} \quad 1 \quad |n| \quad N. \end{cases} \tag{7}$$

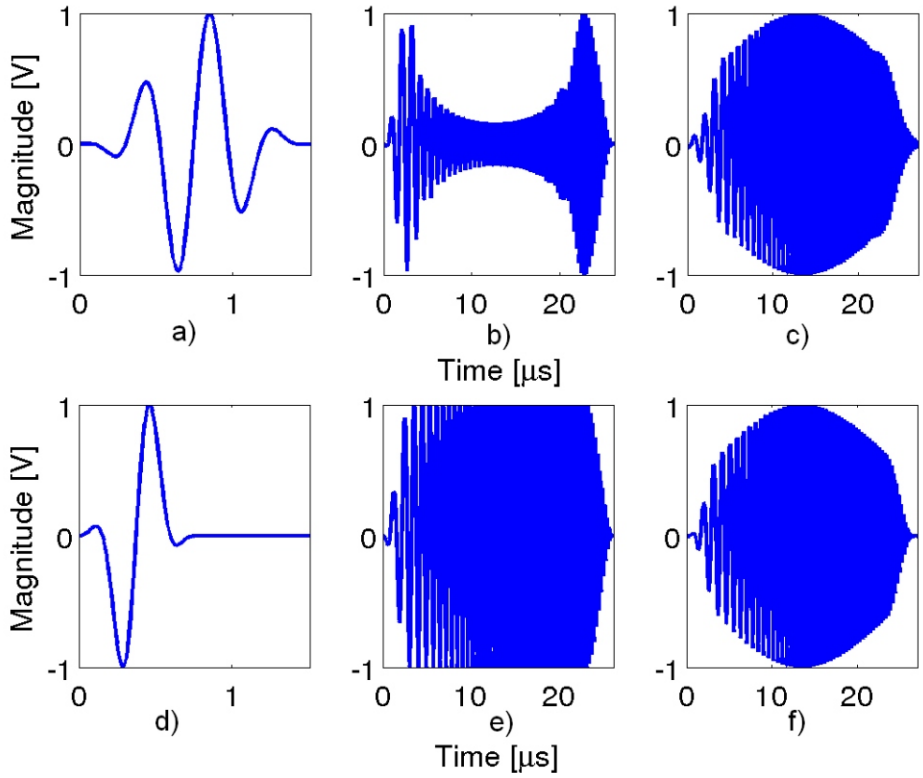


**FIG. 2** Convolution equivalence: a) pulse-echo impulse response with 48% fractional bandwidth, b) pre-enhanced chirp, c) convolution of pulse-echo impulse response and pre-enhanced chirp, d) desired pulse-echo impulse response of 96% fractional bandwidth, e) linear chirp and f) convolution of 96% fractional bandwidth source and the linear chirp.

The parameter controls the amount of taper, which varies from 0 to 1, representing a rectangular window and a Hanning window, respectively. Without a windowing function, the sidelobes approach that of the sinc function at 13 dB. A Hanning window greatly improves sidelobes, i.e., down to 46 dB, but greatly broadens the mainlobe. The Tukey window allows a trade-off between spreading of the main lobe and sidelobe suppression.

To restore the axial resolution, the echo must be postprocessed by pulse compression. The naïve approach to this deconvolution problem is the inverse filter. This approach amplifies noise and is therefore impractical. The matched filter, which maximizes eSNR, suffers from large sidelobes, even as high as 13 dB if not properly constructed. A compromise between inverse filtering and matched filtering is Wiener filtering.[10] Pulse compression in the REC technique was achieved through a Wiener-filter design. The Wiener filter used in the REC technique is given by,

$$_{REC}(f) \quad \frac{V_{LIN}^{*}(f)}{\left|V_{LIN}(f)\right|^{2} \quad \overline{\text{eSNR}}^{\,1}(f)}. \tag{8}$$

The compression filter in Eq. (8) allows a trade-off between gain in eSNR and sidelobe levels. The parameter is a smoothing parameter, a tunable constant that allows the selection of where the filter should operate, i.e., closer to an inverse filter or to a matched filter.

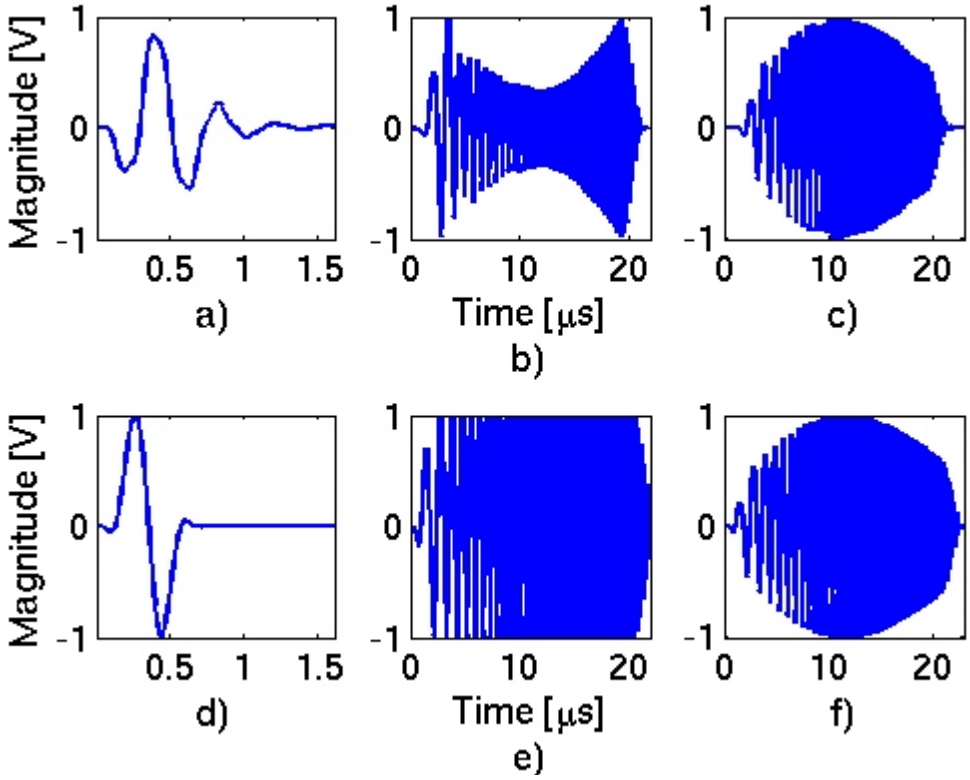


**FIG. 3** a) Pulse/echo impulse response of transducer with $f_0 = 2.35$ MHz and 3 dB fractional bandwidth of 52%, b) pre-enhanced chirp, c) the convolution of the PE/IR (a) and the pre-enhanced chirp b), d) desired pulse/echo impulse response with $f_0 = 2.19$ MHz and a 3 dB fractional bandwidth of 104%, e) linear chirp of optimum bandwidth and f) convolution of desired impulse response d) and linear chirp e).

The $V_{LIN}(f)$ term is the frequency-domain representation of the linear chirp used in the convolution equivalence. The term is a measurement of noise per frequency channel and was estimated by[16]

$$\frac{|H_{2c}(f)|^2 \quad \mathrm{E}\{|\mathrm{F}(f)|^2\}}{\mathrm{E}\{|\ (f)|^2\}}. \tag{9}$$

where $F(f)$ is the object function, $(f)$ is the frequency spectrum of the noise, and $H_{2c}(f)$ is the frequency domain equivalent of

$$h_{2c}(t) \quad \mathrm{E}\ \ \mathrm{g}(t)\,. \tag{10}$$

The parameter $g(t)$ is the compressed signal over noise. Optimal sidelobes and spatial resolution occur when the filter is closer to an inverse filter.

### B. Quality metrics

To evaluate the performance of small-lesion detection using the REC technique, the following image quality metrics were used in simulations and experiments:

*1. Contrast-to-noise ratio (CNR):* CNR is a metric that quantifies the perceived difference between a target image and its background. CNR is defined in this work as[17]

$$CNR \quad \frac{\left|\langle S_i \rangle \quad \langle S_0 \rangle\right|}{\sqrt{\quad {}^2_i \quad {}^2_o}}. \tag{11}$$

where $\langle S_i \rangle$ and $\langle S_0 \rangle$ represent the average intensity inside and outside the target, respectively, and ${}^2_i$ and ${}^2_0$ represent the variance inside and outside the target, respectively. To calculate the CNR, the mean and variance of the signal inside the lesion was estimated by a circular region 90% the size of the lesion. The mean and variance of the background was estimated by calculating the mean and variance of a disk shaped region surrounding the inclusion. A small buffer region between the lesion and background was included to ensure that *only target or background points were included.*

*2. Echo signal-to-noise-ratio (eSNR):* For this work, eSNR was calculated by taking the variance of a collection of points near the focus and dividing it by an estimate of the noise power. The noise power was estimated by taking the variance of the radiofrequency (rf) time signal corresponding to the water bath before the phantom. The assumption here was that the noise power was constant throughout the rf data. The signal variance decayed to the noise variance as samples were taken deeper with respect to axial distance due to attenuation. The eSNR was calculated pre- and postcompression to estimate the gain in eSNR due to the coding technique. Assuming matched filtering, the predicted gain in eSNR relative to pulse compression should be on the order of the time-bandwidth product (TBP).[11]

*3. Resolution cell size*: Wagner et al demonstrated that the average resolution cell size was related to the average speckle cell size.[6] The resolution cell size was estimated from both the physical properties of the transducer and through the characteristics of speckle. The speckle cell size was found through the autocovariance function. Furthermore, the axial speckle cell size is inversely proportional to pulse bandwidth and proportional to transducer beamwidth.[4] Thus, an estimate of the resolution cell volume (axial resolution, $S_{cz}$, and lateral resolution, $S_{cx}$) using 2nd order statistics can be made with the autocorrelation function. The M-point 2-D autocorrelation for a discrete process at lag $k$ and $l$ is represented as[18]

$$R_{ff}(k,l) \quad \sum_{m \ 0}^{M \ 1} f_{m,n} f_{m \ k,n \ l}, \tag{12}$$

where $f_{mn}$ represents the original rf data from the region. The autocorrelation function was applied to a region of speckle adjacent to the lesion in both simulated and experimental data. In the lesion detection simulation and experiments, a 2 2 cm$^2$ square region of interest was used to estimate the resolution cell size from the speckle. The region of interest was located at the focus axially and to the far left of the image laterally. For comparison, an estimate of the resolution cell size in the lateral direction based on the transducer physical properties can be estimated as[19]

$$S'_{cx} \quad \frac{0.87 \ z_0}{d}, \tag{13}$$

where $z_0$ is the distance to the focus, $d'$ the diameter of the transducer divided by 1.08, and is the wavelength of sound in the medium. The substitution $d' = d/1.08$ was recommended by Wagner et al for piston transducers.[6] An estimate of the axial resolution is defined by

$$S'_{cz} \quad \frac{1.37}{f}, \tag{14}$$

where $f$ is the 6-dB bandwidth in MHz and has units of mm.

*4. Lesion signal-to-noise-ratio (lSNR)*: lSNR is an estimate of an isolated observer to detect a lesion and can be estimated by[4]

$$l\text{SNR} \quad \frac{\text{CNR} \quad d}{\sqrt{S_{cx} \quad S_{cz}}}. \tag{15}$$

This metric depends on the lesion diameter, $d$, which is known *a priori* and $S_{cx}$ and $S_{cz}$ are the axial and lateral estimate of the resolution cell volume based on the speckle characteristics. The importance of this metric is that it includes not only the contrast of the lesion but also the ratio of the lesion size to the spatial resolution of the imaging system.

### C. Simulations

Simulations were conducted in MATLAB (MathWorks Inc., Natick, MA) in conjunction with Field II, a MATLAB add-on that simulates ultrasound pressure fields.[19,20] The different excitation schemes were convolved with a theoretical transducer impulse response. The outputs were then normalized to ensure that the peak-pressure amplitudes at the focus of the simulated source were the same between the different excitation schemes. Noise was then added precompression and the coded waveforms were compressed. Three pulsing schemes were compared: conventional pulsing (CP), the conventional linear chirp (LC) and the pre-enhanced chirp (REC).

The simulated source was taken from the actual PEIR of an f/2.66 transducer with a center frequency of 2.35 MHz. The PEIR was estimated by measuring the reflection off of a Plexiglas plate located at the focus. Simulated phantoms were constructed that contained scatterers placed spatially at random positions and uniformly throughout the phantoms at a concentration of 15 scatterers per resolution cell volume. In addition, the mean scattering strength of the scatterers inside the lesion was either 12 dB or +6 dB with respect to the scatterers outside the lesion. Phantoms were simulated with lesion sizes ranging from 1 to 8 mm in diameter in increments of 0.5 mm. Ten phantoms for each lesion size were simulated. The images produced using the three different excitation methods were then compared using CNR, lSNR, eSNR metrics and estimated speckle cell volume based on the autocorrelation function. To estimate the gain in eSNR, both pre- and postcompression estimates of the eSNR were made of the LC and REC waveforms. All rf data were envelope detected with the Hilbert transform and log compressed. The dynamic range for all images was hard limited to 60 dB. Any values lower than 60 dB were truncated to 60 dB. A dynamic range of 60 dB spanned the range of the rf data. A much higher dynamic range, for example, such as 100 dB, would result in a 'washed out' or an overcompressed image. No data would have been lost but the display range would have been over compressed with respect to the dynamic range present in the rf data. The numerical values of the CNR calculations would be different. However, as log compression is a one-to-one mapping function, the overall trends in CNR would be preserved. If the data were compressed on a 30 dB dynamic range, many values in the image would be truncated and set to 30 dB because the rf data had a larger dynamic range than 30 dB. In this case, the image would be corrupted by throwing away too much data. Even so, a CNR value would probably be higher, given that the lesion-to-background strength was less than 30 dB and a 30 dB dynamic range would spread the numerical

values of CNR computed. Adjusting the dynamic range of the 'system' serves as a sort of contrast knob on a television set. The overall trends between the different excitation techniques will be preserved even though a specific value of CNR would be different.

### D. Experimental

The experimental setup included a single-element, weakly-focused (f/2.66) transducer (Panametrics, Waltham, MA). This represents a fixed-focus system. Only images produced near or at the focus are considered in this study. The transducer center frequency (measured) was 2.35 MHz and had a 3-dB pulse-echo fractional bandwidth of 52%. The transducer was mounted on a positioning system that mechanically translated the transducer perpendicular to the major axis of the cone phantom. Two different setups were used: (1) the CP system and( 2) the REC/LC system. Different electronic equipment produced different noise levels. To facilitate a comparison of systems with similar noise levels, the eSNR before compression was normalized to approximately 9.5 dB for both setups. The two different systems are described below.

*1. CP system:* A pulser-reciever (Panametrics 5800, Waltham, MA) was used to excite the transducer and receive the echoes. The echoes were then digitized at 100 MHz with a 12-bit A/D card (Strategic Test Digitizing Board UF3025, Cambridge, MA). All further processing was completed in MATLAB.

*2. REC/LC system:* The excitation waveform was designed in MATLAB and then downloaded to an arbitrary waveform generator (Tabor Electronics W128A, Tel Hanan, Israel) and amplified 50 dB (ENI 3251, Rochester, NY). The amplified signal was passed through a diplexer (Ritec RDX-6, Warwick, RI) to the transducer. As in the CP system, the pulser-receiver was used to receive the echoes before being digitized by the same 12-bit A/D card. All postprocessing was then completed in MATLAB.

The cone-to-background contrast was fabricated to be +6 dB. This contrast was achieved by adding a different concentration of powdered graphite. The compositions of the cone portion of the hydrogel phantom and surrounding medium are shown in tables 1 and 2, respectively. In addition, the speed of sound of the phantom was measured to be 1,540 m/s with an attenuation of 0.49 dB $MHz^{-1}$ $cm^{-1}$.[21] The cone phantom was scanned at slices that corresponded to a lesion diameter of approximately 3, 5 and 8 mm. Two waveforms were transmitted: a pulse and the pre-enhanced chirp (Fig. 3b). The desired impulse response had a center frequency of 2.19 MHz and a 104% 3 dB pulse-echo fractional bandwidth. In this case, the REC technique doubled the fractional bandwidth of the actual impulse response of the transducer. By convolution equivalence in the previous section, figures 3a and 3f should be the same. The REC compression filter is as described in Eq. (8) but the new desired impulse response, figure 3d, was used to create the compression filter. The TBP of the pre-enhanced chirp (Fig. 3b) was 70.3 and the TBP of the linear chirp (Fig. 3e) was 63.4.

Lastly, a LC compression filter was setup to mimic a linear chirp. The rf data that were generated with the pre-enhanced chirp were not only compressed with the REC filter but also with a filter based on the actual excitation signal, i.e., the pre-enhanced chirp. The REC technique requires a boost in bandwidth that is brought about by compression with a higher bandwidth filter. Here, in addition to the REC compression, a compression was also carried out with the original chirp to mimic a conventional pulse compression scheme. This will not give the same boost in resolution but should give a respectable gain in eSNR while approximately maintaining axial resolution. The LC compression filter is as follows,

$$_{LC}(f) \quad \frac{V^{*}_{PRE}(f)}{\left|V_{PRE}(f)\right|^{2} \quad \overline{\mathrm{eSNR}}^{\,1}(f)}, \tag{16}$$

**Table 1** Composition of the cone portion of the hydrogel phantom.[21]

| Material | Composition (%) |
|---|---|
| **Deionized water** | 83.4 |
| **N-propanol** | 9% |
| **Type-A gelatin (Fisher Scientific, Pittsburg, PA)** | 5.5 |
| **Powdered graphite** | 2 |
| **Formaldehyde** | 0.1 |

**Table 2** Composition of the medium surrounding the cone of the hydrodgel phantom.[21]

| Material | Composition (%) |
|---|---|
| **Deionized water** | 84.8 |
| **N-propanol** | 9% |
| **Type-A gelatin (Fisher Scientific, Pittsburg, PA)** | 5.5 |
| **Powdered graphite** | 9.5 |
| **Formaldehyde** | 0.1 |

where $V_{PRE}(f)$ is the frequency domain equivalent of the pre-enhanced chirp and $eSNR^{-1}(f)$ was calculated as in Eq. (10).

## III. RESULTS AND DISCUSSION

### A. Simulations

The gain in eSNR for the two coded methods, LC and REC, were approximately equal: 14.6 and 14.3 dB, respectively. Table 3 lists the eSNR estimates after compression with respect to the three excitation methods. The CP requires no postprocessing and therefore 0 dB gain is reported. The gain achieved for both the LC and the REC technique are dependent on compression filters. The gain was calculated by comparing the eSNR of the precompressed to the compressed B-mode image. The values reported are averages over the 150 simulations.

The estimates of the resolution cell volume based on the speckle analysis are listed in table 4. The REC technique outperformed the other two techniques in the lateral and axial directions. The axial estimate for the REC technique was 0.25 mm compared to 0.33 mm and 0.40 mm for the CP and the LC, respectively. In the lateral dimension, REC achieved 0.78 mm compared to 0.88 mm and 0.97 mm for CP and the LC, respectively. The resolution cell volume and eSNR estimates (Tables 3, 4) have only been reported for the 12-dB simulation. As these metrics are independent of lesion size, similar results are expected for different lesion contrasts

Figures 4a-d shows the results for the two sets of simulations. Figure 4a , b are plots of the CNR and lSNR scores for 150 lesions with a simulated +6 dB lesion-to-background contrast.

**Table 3** Estimated eSNR based on the variance of the speckle at the focus (signal) and the variance of the simulated water bath (noise). Results are averages of 150 simulations.

| Excitation | Average eSNR (dB) | Average Gain (dB) |
|---|---|---|
| **CP** | 17.2 | 0.0 |
| **LC** | 31.8 | 14.6 |
| **EC** | 30.5 | 14.3 |

**Table 4** $S_{cx}$ and $S_{cz}$ estimate of 150 simulated phantoms.

| Excitation | Average $S_{cz}$ (mm) | $S_{cx}$ (mm) |
|---|---|---|
| **CP** | 0.33 ± 0.03 | 0.88 ± 0.09 |
| **LC** | 0.40 ± 0.04 | 0.97 ± 0.10 |
| **REC** | 0.25 ± 0.02 | 0.78 ± 0.08 |

Figure 4c,d are the results of the 150 phantoms with 12 dB lesion-to-background contrast. The +6 dB simulation revealed no best method for increasing the CNR (Fig. 4a). However, the gains in resolution resulted in higher lSNR values compared to CP and the LC for all lesion sizes (Fig. 4b). The numerator of the lSNR function includes an estimate of the CNR and the diameter of the lesion. The denominator contains an estimate of the resolution cell volume. Thus, it is expected for the lSNR to tend toward zero as the lesion becomes smaller. The results of the CNR from the simulated lesions of 12 dB contrast are given in figure 4c. The CNR values obtained using the REC technique were higher than the CNR values estimated for CP and LC for all lesions greater than 2 mm in diameter. However, observation of the curves in figure 4a suggests that the behavior of the CNR estimate may become more erratic at smaller lesion sizes. In all cases, the lSNR was higher for the REC technique compared to the other techniques (Fig. 4b). B-mode images of the 5-mm lesion for the three excitation types and contrast types are shown in figure 5 and figure 6. The B-mode images show that the REC technique improved spatial resolution by the smaller speckle size apparent in the axial direction.

The erratic CNR curves for the smaller lesions suggested that the number of image samples available for the CNR calculation for small lesions may be too low to achieve good accuracy and precision compared to larger lesions. The CNR quality metric includes the variance of the area inside and outside the inclusion. As the inclusion becomes smaller, there are also fewer data points to make an accurate estimate of the variance of the target region. It is presumed that a certain number of independent samples are needed before an accurate estimate can be obtained. The bias and variance of the CNR estimate may also be a function of the resolution cell volume. For a given region-of-interest size used to calculate CNR, a better spatial resolution should lead to an improved CNR estimate.

The dependence of the CNR calculation on the region-of-interest size and the spatial resolution were examined using simulations. Ten simulated phantoms were generated with 15 scatterers per resolution cell placed spatially at random. A simulated lesion of 8-mm diameter was positioned at the center of the phantoms with mean scatterer strength of 12 dB with respect to the background scatterer strength. Using Field II, an f/3 transducer was translated

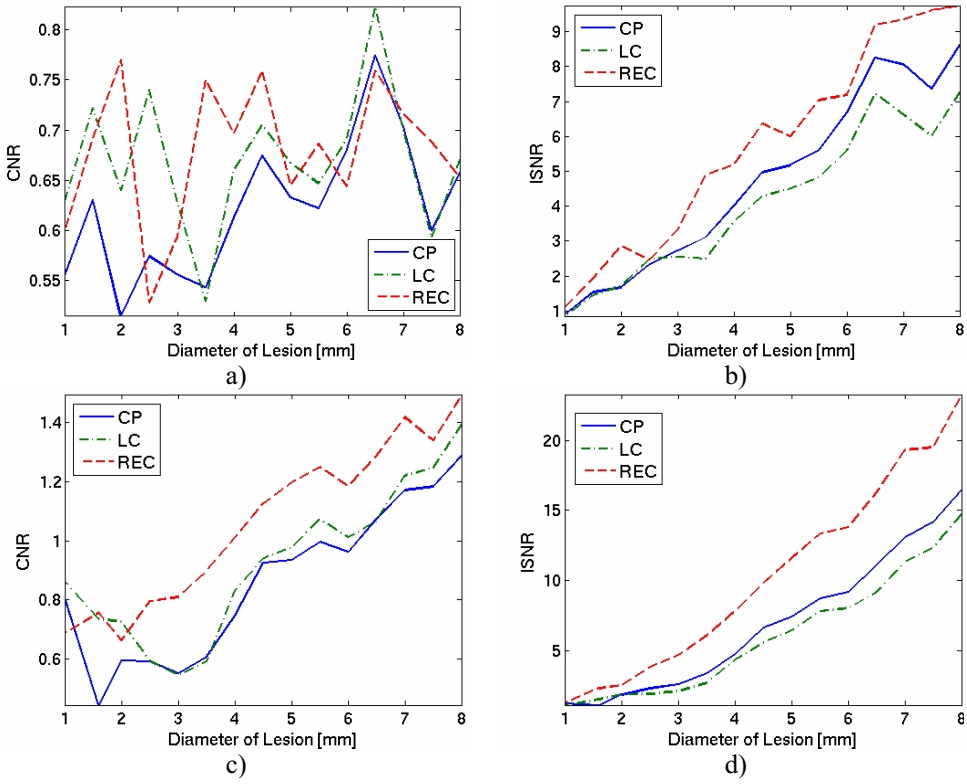


**FIG. 4** Simulation results for the +6 dB and -12 dB contrast lesions. a) CNR of the +6 dB contrast lesions, b) lSNR of the +6 contrast lesion, c) CNR of the 12 dB contrast lesion and d) lSNR of the 12 dB contrast lesion.

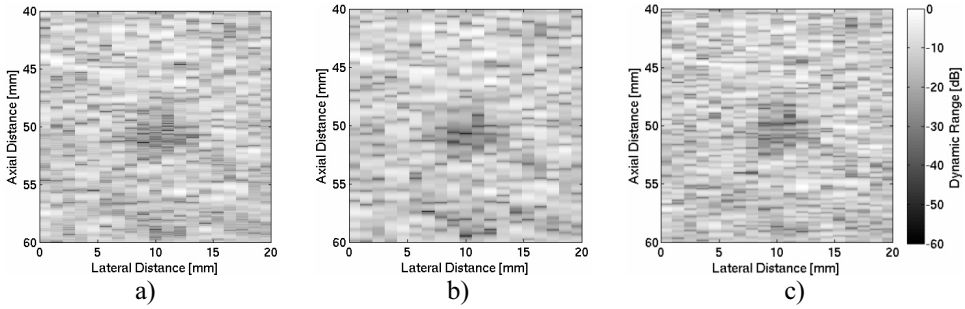


**FIG. 5** 5-mm lesion with 12 dB contrast (displayed with 60 dB dynamic range). a) CP, b) LC and c) REC.

laterally with half a beamwidth overlap to generate rf data. Field II also allows the impulse response of the transducer to be set. In this simulation, the pulse/echo impulse response was a sinusoid centered at 2.25 MHz and windowed with a Blackman window. The 3 dB pulse-echo fractional bandwidth of the transducer was 48%.

To test the dependence of CNR on pulse length, excitation of a pulse (CP), single cycle, two cycle and four cycle sinusoids centered at 2.25 MHz were tested. Rf data of the ten phantoms imaged with these four excitation schemes were generated. The CNR was then calculated in regions ranging from approximately 6% to 100% of the size of the lesion which corresponded to 24 -7,500 data points, respectively. The CNR variance of the different excitation methods as a function of the number of data points is diplayed in figure 7a. From fig-

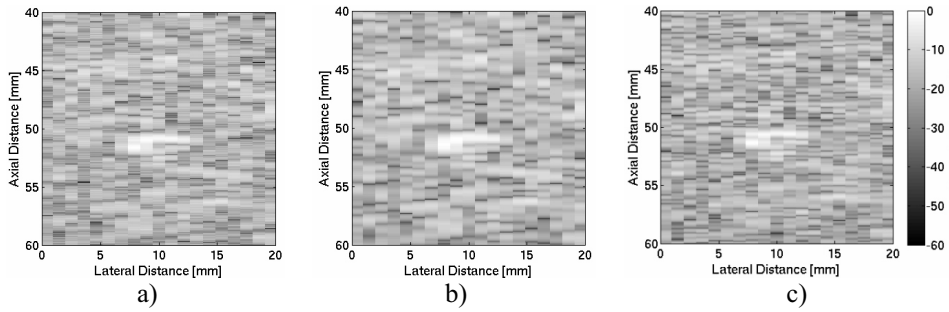


**FIG. 6** 5-mm lesion with +6 dB contrast (displayed with 60 dB dynamic range). a) CP, b) LC and c) REC.

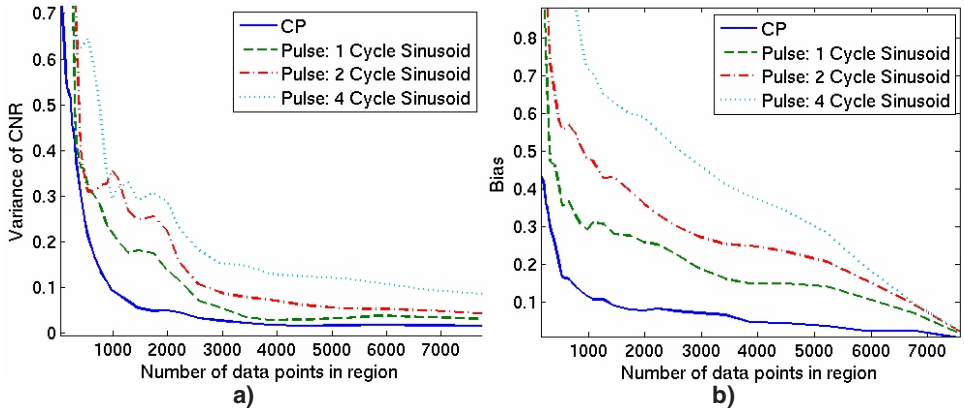


**FIG. 7** Results of 10 simulated phantoms. a) variance of CNR versus number of data points used to calculate variance of region and b) bias estimate for Field II simulations.

ure 7b, the number of data points needed before an estimate with a bias less than 0.1 could be acquired was greater than 3,000 for CP. Therefore, if the size of the lesion is too small relative to the spatial resolution of the imaging system, the accuracy and precision of the CNR and lSNR estimates degrade. Furthermore, the results suggest that fewer samples are needed for CNR calculations for shorter-duration pulses. Fewer samples are needed to get a good estimate of CNR with shorter pulses, i.e., larger bandwidth, because for samples coming from a region of specified size, shorter pulses result in more independent samples in the region. Improving the axial resolution of an imaging system should lead to better CNR estimates for smaller samples sizes.

## B. Experimental

The theoretical resolution from the transducer properties and estimated resolution cell size from the speckle analysis are reported in table 5. A gain in lateral and axial resolution was achieved using REC. The axial resolution of REC (0.21 mm) outperformed the other two techniques (0.28 mm) of CP and the LC. Unexpectedly, the lateral resolution estimate for REC (1.35 mm) also improved over the other two methods (1.7 mm). The eSNR values and the gain in eSNR from compression for all techniques are listed in table 6. The TBP of the excitation waveform was 40, so the expected gain in eSNR would be approximately 16 dB. However, this gain is the best estimate for the matched filtering case. The LC compression filter has been tuned closer to a matched filter than the REC technique, which produces a

**Table 5** Lateral and axial speckle cell volume estimate of experimental phantom.

| Excitation | $S'_{cx}$ (mm) | $S'_{cz}$ (mm) | $S_{cx}$ (mm) | $S_{cz}$ (mm) |
|---|---|---|---|---|
| **CP** | 1.6 | 0.80 | 1.70 | 0.28 |
| **LC** | 1.6 | 0.80 | 1.70 | 0.28 |
| **EC** | 1.6 | 0.40 | 1.35 | 0.21 |

**Table 6** Experimental results for eSNR(dB) and gain(dB).

| Diameter | 3 mm | | 5 mm | | 8 mm | | Average | Average |
|---|---|---|---|---|---|---|---|---|
| **Excitation** | **eSNR** | **Gain** | **eSNR** | **Gain** | **eSNR** | **Gain** | **eSNR** | **Gain** |
| **CP** | 9.08 | 0 | 9.35 | 0 | 9.43 | 0 | 9.29 | 0 |
| **LC** | 19.92 | 10.9 | 21.53 | 11.0 | 19.61 | 10.2 | 20.4 | 10.7 |
| **EC** | 15.08 | 6.0 | 14.80 | 4.2 | 16.42 | 6.7 | 15.4 | 5.7 |

higher eSNR gain at the expense of axial resolution (10.66 dB average gain and 0.28 mm axial resolution with LC versus 5.74 dB gain and 0.21 mm axial resolution with REC).

The experimental data consisted of three slices perpendicular to the main axis of the cone phantom. The phantom was scanned at slices corresponding to a cone diameter of 3, 5 and 8 mm. The noise power was estimated by taking the variance of the signal corresponding to the water bath before the phantom. The signal power from the scatterers was estimated by taking the variance of a line of speckle along the axial direction at the depth of the lesion (68 cm).

The 5-mm B-mode image of the three excitations types is displayed in figure 8. The number of data points used for calculation of CNR and lSNR for the 3-mm lesion was 3,262 points. As found previously, the lack of sample points may result in less reliable estimates of CNR. The number of points used in the 5-mm and 8-mm lesion was 9,123 and 23,429, respectively. The CNR and lSNR values for all cases are listed in table 7. The CNR for REC outperformed the LC and CP in the detectability of the 5-mm and 8-mm lesions. The poor performance in the 3-mm case with respect to REC and CNR could be attributed to a lack of sufficient data points. In addition, small sample size could also be an issue (one cone phantom). However, the lSNR metric was higher for REC even though the CNR score was lower in the 3-mm case. This can be attributed to the significant increase in axial resolution achieved with the REC technique. That increase in resolution dominated the REC lSNR score. The lSNR score was boosted by 15%, 45% and 40% for the 3, 5 and 8-mm lesions respectively.

## IV. CONCLUSION

The ability of an ultrasonic imaging system to detect focal lesions against a background is of paramount importance. Of special interest is the detection of small, low contrast targets because this is one of the practical limitations of an ultrasonic imaging system. ROC curves

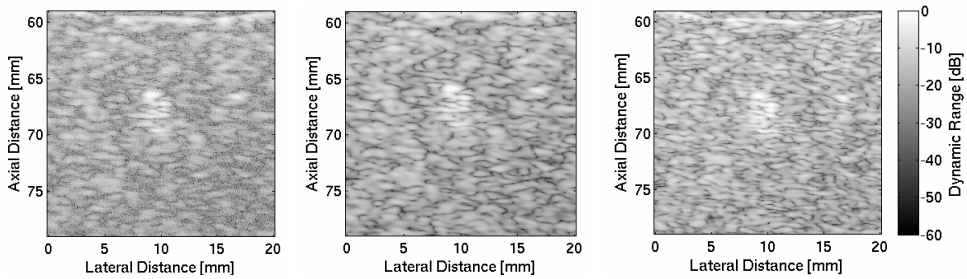


**FIG. 8** The 5-mm slice (displayed with 60 dB dynamic range). a) CP, b) LC and c) REC.

**Table 7** Experimental results for CNR and lSNR.

| **Diameter** | **3 mm** | | **5 mm** | | **8 mm** | |
|---|---|---|---|---|---|---|
| **Excitation** | **CNR** | **lSNR** | **CNR** | **lSNR** | **CNR** | **lSNR** |
| **CP** | 1.41 | 6.14 | 1.06 | 7.67 | 90.80 | 9.22 |
| **LC** | 1.32 | 5.80 | 1.13 | 8.30 | 0.93 | 10.34 |
| **EC** | 1.26 | 7.08 | 1.29 | 12.05 | 0.97 | 14.50 |

take months to generate and require clinicians, ground truth and histology to formulate. Contrast/detail analysis is a way to quickly evaluate an imaging system's performance on small, low contrast targets. The lSNR is a metric that combines CNR, resolution cell size and the diameter of a lesion to provide information for lesion detectability of an imaging system. The lSNR metric allows the primary evaluation of an imaging system or modification to an imaging system without the effort involved in providing ROC curves.

The REC technique improved lesion detectibility for all of the simulated and experimental cases. In experiments, the lSNR was increased by 16%, 56% and 32% for the 3, 5 and 8 mm lesions, respectively. The low estimate of CNR for the 3-mm-diameter phantom in the experimental case may be due to a poor estimate because of a low number of samples available. Even so, the boost in bandwidth by the REC technique improved lSNR for the 3-mm case. Therefore, according to the lSNR metric, the REC technique improved the performance of the ultrasonic imaging system to detect small lesions. This may have significance for medical diagnostics. However, only a fixed-focus system has been considered. Of interest is the effect of REC on a dynamic-focus system; this may be explored in future studies.

The REC technique also improved eSNR while boosting the axial resolution over the conventional pulsing technique. The REC technique boosted energy in transition bands of the transducer, which, in turn, increased the usable bandwidth of the transducer. The increase in the usable bandwidth resulted in an improved axial resolution. That is, at the same eSNR, the REC filter should be able to operate closer to an inverse filter, improving axial resolution.

## ACKNOWLEDGMENTS

The authors would like to thank the technical assistance of Marko Orescanin in the construction of the cone phantom. This work was supported by a grant from the NIH (R21EB006741).

## REFERENCES


1. Smith S, Lopez H. A contrast-detail analysis of diagnostic ultrasound imaging, *Med Phys 9,* 4-12 (1982).

2. Szabo T. *Diagnostic Ultrasound: Inside Out* (Elsevier Inc, Burlington, MA, 2004).

3. Lizzi F, Greenebaum E, Feleppa E. Theoretical framework for spectrum analysis in ultrasonic characterization, *J Acoust Soc Am 73,* 1366-1373 (1983).

4. Smith SW, Wagner RF, Sandrik JM, Lopez H. Low contrast detectability and contrast/detail analysis in medical ultrasound, *IEEE Trans Sonics Ultrason 30,* 164-173 (1983).

5. Bamber JC. Speckle reduction, in *Advances in Ultrasound Techniques and Instrumentation, Clinics in Diagnostic Ultrasound,* Vol. 28, pp. 55-67 (Churchill Livinstone, New York, 1993).

6. Wagner RF, Smith SW, Sandrik JM, Lopez H. Statistics of speckle in ultrasound B-scans, *IEEE Trans Sonics Utrason 30*, 156-163 (1983).

7. Nathanson FE. *Radar Design Principles,* 2nd ed. (McGraw-Hill, New York, 1991).

8. Takeuchi Y. An investigation of a spread energy method for medical ultrasound systems part one: theory and investigation, *Ultrasonics,* 175-182 (1979).

9. Misaridis T, Jensen JA. Use of modulated excitation signals in medical ultrasound. part II: design and performance for medical imaging applications, *IEEE Trans Ultrason Ferroelectr Freq Contr 52,* 192-207 (2005).

10. Misaridis T, Jensen JA. Use of modulated excitation signals in medical ultrasound. part I: basic concepts and expected benefits, *IEEE Trans Ultrason Ferroelectr Freq Control 52,* 177-191 (2005).

11. Haider B, Lewin PA, Thomenius KE. Pulse elongation and deconvolution filtering for medical ultrasonic imaging, *IEEE Trans Ultrason Ferroelectr Freq Cont 45*, 98-112 (1998).

12. Oelze ML. Bandwidth and resolution enhancement through pulse compression, *IEEE Trans Ultrason Ferroelectr Freq Contr 54,* 768-781 (2007).

13. Sanchez J, Oelze ML. An ultrasonic imaging speckle-suppression and contrast enhancement technique by means of frequency compounding and coded excitation, *IEEE Trans Ultrason Ferroelectr Freq Contr 56,* 1327-1339 (2009).

14. Sanchez J, Oelze ML. A novel coded excitation scheme to improve spatial and contrast resolution of quantitative ultrasound imaging, *IEEE Trans Ultrason Ferroelectr Freq Contr 56,* 2111-2123 (2009).

15. Pollakowski M, Ermert H, Bernus L, et al. The optimum bandwidth of chirp signals in ultrasonic applications, *Ultrasonics 31,* 417-420 (1993).

16. Tsou JK, Liu J, Insana MF. Modeling and phantom studies of ultrasonic wall shear rate measurements using coded pulse excitation, *IEEE Trans Ultrason Ferroelectr Freq Contr 53,* 724-734 (2006).

17.Dahl JJ, Guenther DA, Trahey G. Adaptive imaging spatial compounding in the presence of aberration, *IEEE Trans Ultrason Ferroelectr Freq Contr 52,* 1131-1144 (2005).

18. Cobbold RSC. *Foundations of Biomedical Ultrasound* (Oxford University Press, New York, 2007).

19. Jensen JA. Field: a program for simulating ultrasound systems, *Med Biol Eng Comp, Suppl 1, 34,* 351-353 (1996).

20. Jensen JA, Svendsen NB. Calculation of pressure fields from arbitrarily shaped, apodized, and excited ultrasound transducers, *IEEE Trans Ultrason Ferroelectr Freq Control 39,* 262-267 (1992).

21. Sanchez J. *Improving Ultrasonic Imaging Using Novel Coded Excitation,* Doctoral Dissertation (Dept. of Electrical and Computer Engineering, University of Illinois, Urbana, IL, 2010).